Designing Indigo-based HTMs for Sn-Perovskite Photovoltaics: A Computational Approach

by

Dias Mustazheb

B.Sc., Nazarbayev University

Thesis Submitted in Partial Fulfillment of the Requirements for the Degree

of Master of Science in Chemistry

at Nazarbayev University

Supervisor: Dr. Mannix P. Balanay

2023

Abstract

Indigo-based structures were designed with the help of density-functional theory (DFT) and

proposed as potential hole-transporting materials (HTMs) for tin-based and mixed-metal perovskite solar cells (PSCs). First, theoretical methodology was benchmarked to determine the most appropriate functionals for optimization and calculation of the energies of indigo-based structures, using reference structures with known energies. A linear mathematical model was built based on calculations of reference structures, to estimate and predict actual energy levels of indigo-based molecules. It was shown that GSOPv is a good estimation of actual HOMO energy for indigoid structures. Next, the influence of position of attachment of new substituents on the final HOMO energy was studied and used for design of new structures. Indigoids with alkoxy and alkylamine groups attached at 5,5'- positions, as well as asymmetric structure with cyclic and alkylamine groups attached, were demonstrated to have suitable energetics for application as HTMs for $CsSnI_3$ and $MASn_{0.5}Pb_{0.5}I_3$ PSCs.

Table of Contents

List of abbreviations

PSC perovskite solar cell

PCE power conversion efficiency

ETM electron transport material

HTM hole-transporting material

Spiro-OMeTAD 2,2',7,7'-tetrakis-(*N,N*-di-4-methoxyphenylamine)-9,9'-spirobifluorene DFT density functional theory

TD-DFT time-dependent density functional theory

TFSI bis(trifluoromethanesulfonyl)imide

TBP *tert*-butylpyridine

HOMO highest occupied molecular orbital

LUMO lowest unoccupied molecular orbital

GSOP ground state oxidation potential

ESOP excited state oxidation potential

MAE mean absolute error

MSE mean square error

List of Figures

List of Tables

1. Introduction

With the ever-increasing consumption of electricity, more and more sources of energy must be developed to meet demand. Fossil fuels are not environmentally friendly because their use releases CO_2, a major greenhouse gas that contributes to the worldwide problem of global warming. To meet energy demand and curb global warming, environmentally friendly and renewable energy solutions must be developed. One of the possible solutions is solar energy conversion technologies, because solar energy is absolutely environmentally friendly and renewable.

Perovskite solar cells (PSCs) are one of the latest hot topics in solar energy conversion. Since the first PSC was reported in 2009 [1], they have attracted the attention of the scientific community around the world, leading to an enormously rapid improvement in their design and performance,

which has already reached a power conversion efficiency (PCE) of 25.8%[2]. However, there are some problems that hinder their commercialization. One problem is the toxicity of lead, which is commonly used in PSCs. To solve this problem, lead-free PSCs are currently being developed, such as those based on tin, and mixed-metal PSCs with lower lead content are also a good alternative. Another major source of problems is the hole transport material (HTM) used in PSCs. Spiro-OMeTAD is an organic HTM most commonly used in PSCs. However, due to its structure, its synthesis is complicated and therefore quite expensive, which increases the cost of PSCs. In addition, there are problems with the long-term stability of spiro-OMeTAD. To solve these problems, intensive research is being conducted to replace spiro-OMeTAD with another material that is cheaper and does not affect the long-term stability of PSCs.

One approach to developing new materials with desired properties is to use computational methods. Computational methods such as density functional theory (DFT) and time-dependent density functional theory (TD-DFT) allow the simulation of new molecules and the prediction of their properties, making the screening of new materials for desired properties cheaper and faster. In this work, methods based on DFT are used to develop new indigo-based hole transport materials for lead

free and mixed-metal perovskite solar cells.

2. Literature Review

2.1. Perovskite Solar Cells

Perovskite materials have the general formula ABX_3, where A and B are cations and X is an anion; a unit cell of perovskite is shown in **Figure 1**. These structures have unique semiconducting and optical properties, such as long carrier diffusion lengths, and are easy to synthesize, promising great potential for applications in electronics, optoelectronics, and nonlinear optics [3,4].

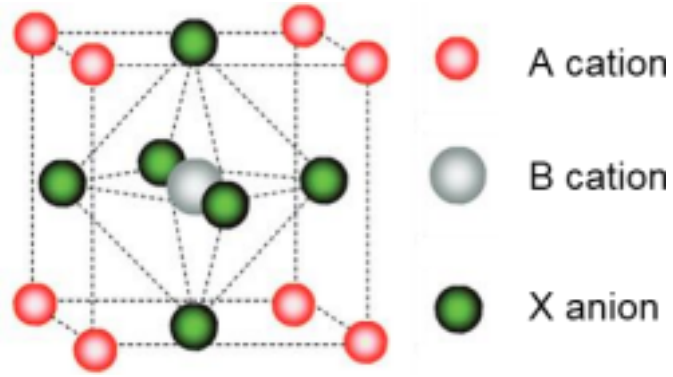

Figure 1. Crystal structure of perovskite ABX_3.

The first publication showing the successful application of perovskites for solar energy conversion was in 2009, when Kojima *et al.* reported the use of organic-inorganic lead halide perovskites $CH_3NH_3PbBr_3$ and $CH_3NH_3PbI_3$ as photosensitizers instead of organic dyes in a dye sensitized solar cell (DSSC) [1]. Particles of nanocrystalline perovskites were deposited on the surface of a mesoporous TiO_2 layer on a glass substrate coated with fluorine-doped tin oxide (FTO). This working photoelectrode (anode) was fused to a counter electrode of Pt-coated FTO glass (cathode). The gap between the two electrodes was filled with a liquid electrolyte solution, which transported the electrons from the counter electrode back to the perovskite sensitizer. At that time, an efficiency of 3.81% was achieved. However, there was a serious problem with the liquid electrolyte, as the perovskite crystals dissolved in it. This made it difficult to produce cells stable enough to measure their PCE, let alone operate them over the long term [4]. To overcome this problem, a solid-state device had to be developed that contained a solid hole transport material (HTM) instead of a liquid electrolyte.

The first solid-state PSC was published in 2012 by Kim *et al.* [5] they replaced the liquid electrolyte with a solid-state HTM of organic 2,2',7,7'-tetrakis-(*N,N*-di-4-methoxyphenylamine)-9,9'-spirobifluorene (spiro-OMeTAD). This solved the problem of dissolution of the perovskite. Since

then, spiro-OMeTAD has been the most commonly used HTM for PSCs. They also varied the thickness of the mesoporous TiO_2 layer and showed that better performance can be achieved with thinner layers. The best PCE of 9.7% was achieved with a TiO_2 layer thickness of 0.6 μm. This was the first indication of differences in the operating mechanism between PSCs and DSSCs.

In the same year, Lee *et al.* replaced the mesoporous TiO_2 layer with a mesoporous Al_2O_3

layer that served as an inert framework for the deposition of perovskite and improved the PCE to 10.9%[6]. This shows that, unlike DSSCs, a thick layer of mesoporous TiO_2 is not required for efficient charge transport because electrons can be transported through the perovskite layer itself. This means that perovskite is not a sensitizer, but itself an intrinsic semiconductor capable of charge transport. This makes it possible to develop planar thin-film PSCs in which the perovskite absorber layer is sandwiched between thin layers of selective p- and n-contacts.

Further research on the fabrication of thinner PSCs led to the first planar heterojunction PSC that does not use a mesoporous framework. Liu *et al.* reported this in 2013 [7]. The authors stacked the thin perovskite layer on top of the compact TiO_2 layer. They achieved the highest PCE of 15.4%. Since then, planar PSCs have been developed at a rapid pace and now achieve a PCE of 25.8% [2].

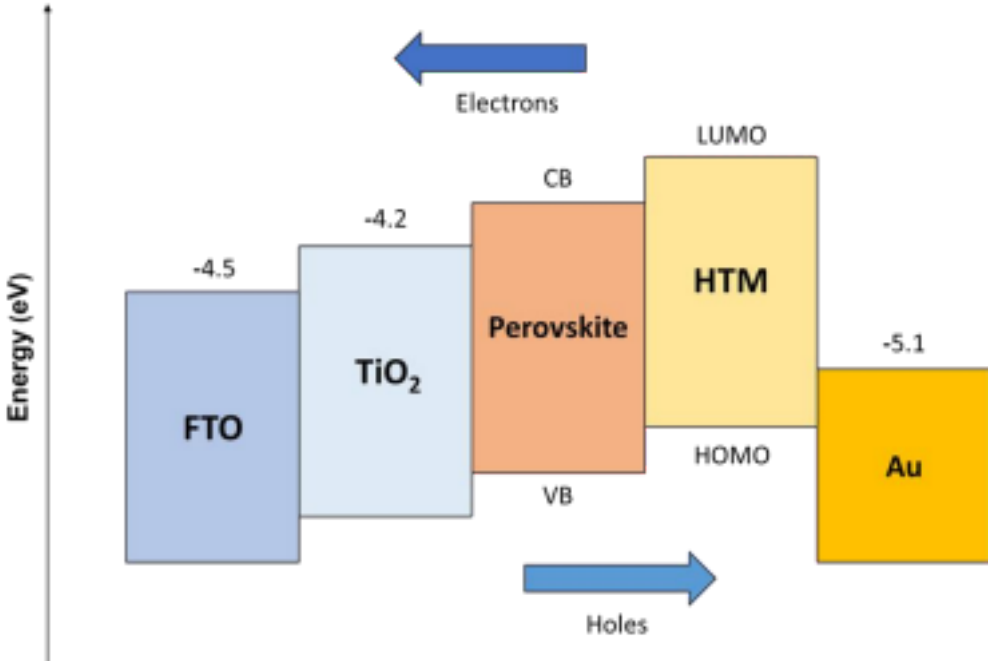

Figure 2. Schematic representation of a perovskite solar cell.

The above results provided a better understanding of the functional mechanisms of PSCs, which are schematically shown in **Figure 2**. Unlike dyes in DSSCs, perovskites are intrinsic semiconductors. Absorption of sunlight creates electron-hole pairs in the bulk of the perovskite, where they can diffuse in either direction. On one side, the n-type contact, which consists of a layer of electron transport material (ETM), usually compact TiO_2, only collects electrons and transfers them to the external circuit through the FTO glass. On the other hand, the layer of p-type hole

transport material (HTM) collects only holes and transfers them to the external circuit through the gold electrode.

Another major problem with PSCs is the use of lead-based perovskites, which pose many problems with the safety of their use. Lead and its compounds are very toxic, directly affecting the nervous and hematopoietic systems and causing cardiovascular damage. It is practically impossible to completely remove or reverse the damage caused by lead poisoning from the organism [8].

Therefore, it is important to find alternatives that can replace lead in the perovskite structure while maintaining excellent photovoltaic properties. Tin-based perovskites, such as $CH_3NH_3SnI_3$ ($MASnI_3$) [9,10] and $CsSnI_3$ [11,12] , have been proposed as alternatives to lead-based perovskites because Sn is similar to Pb in size and valence and therefore should have the same crystal structure and optoelectronic properties. However, Sn(Ⅱ) is unstable and easily oxidizes to Sn(Ⅳ), so Sn-based perovskites are very susceptible to air and moisture, which affects the active layer and solar cell performance [10]. An alternative approach is to minimize the Pb content instead of eliminating it completely by mixing Pb and Sn. This stabilizes Sn(Ⅱ) and improves safety over Pb-based PSCs and performance over Sn-based PSCs. If Pb and Sn are mixed in equal amounts, the mixed perovskite $MASn_{0.5}Pb_{0.5}I_3$ will be obtained, which has an even smaller band gap and higher short-circuit photocurrent than the normal $MAPbI_3$ or its tin analogue $MASnI_3$ [13].

2.2. Hole-Transporting Material

Since the first report in 2012 [5] , Spiro-OMeTAD (2,2′,7,7′-tetrakis(N,N-di-p methoxyphenyl-amine)9,9′-spirobifluorene) has been the most popular solid HTM used in PSCs. However, its use leads to certain limitations in the commercialization of PSCs. Due to its structure (**Figure 3**), it is difficult to synthesize and quite expensive. In addition, the poor long-term stability of PSCs is often associated with the use of spiro-OMeTAD as HTM. In particular, the stability problems are related to the presence of Li-TFSI (Lithium bis(trifluoromethanesulfonyl)imide) and TBP (*tert*-

butylpyridine) dopants in spiro-OMeTAD-based HTMs. The dopants are added to increase the hole mobility of spiro-OMeTAD because the hole mobility of pure spiro-OMeTAD is not high enough to be an effective HTM [14]. TBP degrades spiro-OMeTAD and perovskite layers in the long term, while lithium cations can migrate through the HTM and perovskite layers, affecting cell performance

[4]. One way to solve the stability problem is to replace the dopants. For example, Seo *et al.* replaced Li-TFSI with Zn-TFSI2, which reduced the migration of cations due to the larger size of Zn^{2+} ions and achieved better PCE and thermal stability [15]. However, stability problems still occurred at an elevated temperature of 50°C, as well as problems related to the TBP additions. Moreover, the change of dopants does not solve the problem of complicated synthesis and high cost of spiro-OMeTAD.

Figure 3. Structures of (a) spiro-OMeTAD and dopants: (b) Li-TFSI and (c) TBP.

Another way to address these issues is to develop alternative, preferably doping-free HTMs to replace Spiro-OMeTAD. To function as an effective HTM, the new material must meet several requirements. The most important properties are related to the energetics of the material. To successfully collect holes and transfer them to gold, as shown in **Figure 2**, the energy level of the material with the highest occupied molecular orbital (HOMO) should be higher than the valence band of the perovskite layer and lower than the conduction band of Au. Otherwise, the transfer of holes from perovskite to HTM and then to Au is energetically unfavorable. At the same time, the energy level of the lowest unoccupied molecular orbital (LUMO) of HTM should be higher than the conduction band of perovskite, so that it acts as an energy barrier and blocks the flow of electrons in the opposite direction. In addition, the new HTM should have high hole mobility to increase current flow, and it should be stable to air and moisture.

Immediate candidates for alternative HTMs are conductive organic polymers. In 2013, Cai *et al.* reported the use of the diketopyrrolopyrrole (DPP)-based polymer PCBTDPP (poly[N-90-heptadecanyl-2,7carbazole-alt-3,6-bis(thiophen-5-yl)-2,5-dioctyl-2,5-dihydropyrrolo[3,4]pyrrole

1,4-dione]) as a new HTM [16]. In 2014, Ryu *et al.* fabricated PSCs using a PTAA (poly[bis(4-phenyl)(2,4,6-trimethylphenyl)amine]) polymer as HTM [17]. An efficiency of 16.2% was achieved using $MAPbI_3$ perovskite. In 2015, Heo *et al.* used PEDOT:PSS (poly(3,4-ethylenedioxythiophene):polystyrene sulfonate) as HTM in inverted planar PSCs and achieved a PCE of 18.1% and lower hysteresis than PSCs with doped PTAA as HTM [18]. Recently, in 2018, Cai *et al.* reported the design of π-π-stacked conjugated polymers as novel HTMs for PSCs [19]. The authors designed benzothiadiazole-based donor-acceptor copolymers. The best of them, PCDTBT1 (poly[N 9′′-hepta-decanyl-2,7-carbazole-alt-5,5-(4′,7′-di-2-thienyl-2′,1′,3′-benzothiadiazole)]), contributed to achieve a PCE of 19.1%. In addition to conducting polymers, dopant-free molecular HTMs are also of interest. Recently, in 2020, Jiang *et al.* fabricated PSCs with HTM from tetraphenylethylene-based TPE-S [20]. The new PSCs achieved a PCE value of 15.4%, which was higher than the 12.0% of the reference PSCs based on PEDOT:PSS. Despite all the progress in the development of alternative HTMs, spiro-OMeTAD remains the most popular HTM, as the recently published PCE record of 25.8% was also achieved with PSCs containing spiro-OMeTAD [2].

2.3. Computational Design of HTMs

One approach to developing new materials with desired properties is to use computational methods. Computational methods such as density functional theory (DFT) and time-dependent density functional theory (TD-DFT) make it possible to simulate new molecules and predict their properties. This makes screening new materials for desired properties cheaper and faster.

One of the first papers using purely computational methods to study the properties of novel HTMs was published in 2015 by Wei-Jie Chi and Ze-Sheng Li. In it, they designed six different molecules (**Figure 4**) with different electron donating groups attached to the 4-(4-phenyl-4-α naphthylbutadieny)-triphenylamine scaffold [21]. The authors used DFT methods to optimize the ground state geometries of the molecules and obtain their HOMO and LUMO energies. TD-DFT The calculations were used to obtain absorption and emission spectra of the molecules. Also, the reorganization energies of holes and electrons were calculated using the theoretical electron energies. It was found that the introduction of electron donating groups HOMO and the LUMO energies of the

molecules increased and became less negative, and the effect increased with the electron donating

ability. At the same time, the effect is smaller for LUMO than for HOMO, suggesting that electron donating groups make the molecules more effective hole transporters than electron transporters. This is also supported by the observation that the HOMOs of the molecules are more delocalized throughout the structure than the LUMOs, which are often localized on one half of the structure.

Finally, it was calculated that the reorganization energies of the holes are lower than the reorganization energies of the electrons, suggesting higher mobility of the holes. Therefore, the proposed molecules are better hole transporters than electron transporters.

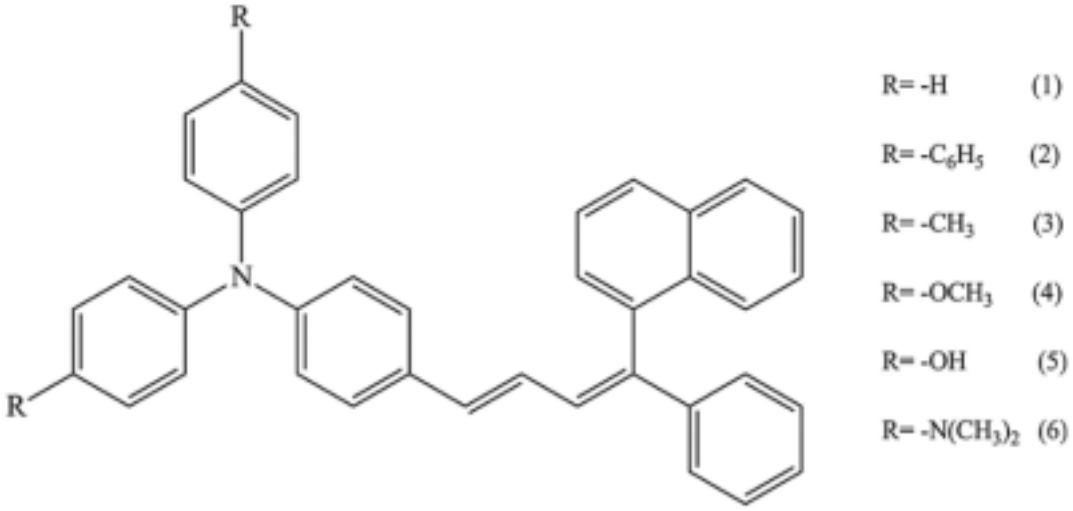

Figure 4. Novel HTM structures based on 4-(4-phenyl-4-α-naphthylbutadieny)-triphenylamine [21].

One of the problems with the methodology of the paper is that the authors used only the B3LYP functional for the geometry optimization and the CAM -B3LYP functional for the TD-DFT calculations. In addition, few experimental reference data were used to evaluate the accuracy of the theoretical methods. Specifically, there were experimentally measured data for two of six molecules, which does not allow for a proper evaluation of the accuracy of the method. Using these two molecules, it was shown that the theoretical models have limited accuracy, with absolute errors in the calculated HOMO and LUMO energies of up to 0.94 eV. However, correlation of the theoretical and experimental data was not performed and was not possible. For this reason, different functionals could not be evaluated to find the most accurate one, and the actual energies of the molecules could not be derived from the theoretical values. Overall, the theoretical methodology was not optimized. Nevertheless, the work has shown that computational methods can be used to evaluate HOMO and

LUMO of the molecules of interest and provide valuable insight into the effects of electron donating

groups on the energetics of the molecules.

A more thorough optimization of the methodology was performed in the work of Gapol *et al.* published in 2017 [22] The authors investigated tetraphenylbenzidine (TPB)-based structures with different electron-withdrawing and electron-donating groups. However, before that, several experimentally already characterized reference molecules with similar TPB structures were used to evaluate different DFT functionals and select the most accurate one. Five DFT functionals and three TD-DFT functionals were used to calculate the energies of the reference molecules. The ground state oxidation potential (GSOP) and excited state oxidation potential (ESOP) values were also calculated. In previous work [23] , it was reported that the theoretical HOMO energies of dyes have large errors, while the calculation of GSOP leads to a more accurate estimate of the experimental HOMO. ESOP is obtained by adding the first excitation energy (E_1) from the TD-DFT calculation to GSOP. The theoretical data were then compared and correlated with experimental data available for reference molecules. In this way, the functional with the best correlation to the experimental data can be determined and used for further calculations of novel HTMs.

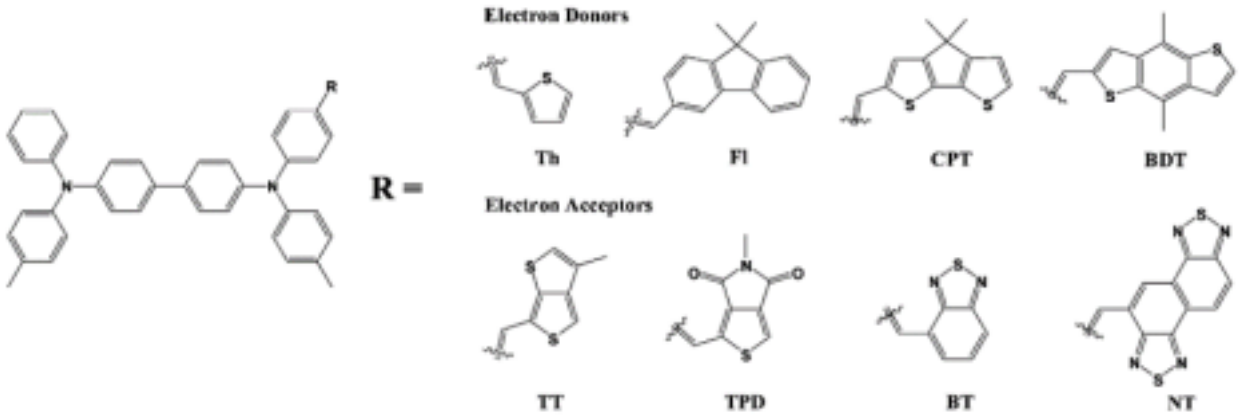

Figure 5. Tetraphenylbenzidine (TPB)-based structures of novel HTMs. [22]

Comparison of the theoretical and experimental data showed that the GSOP values are indeed closer to the experimental HOMO energies than to the theoretical HOMO energies. It was found that LC -ωPBE is the best functional for geometry optimization and GSOP calculation of TPB-based molecules. Similarly, the B3LYP functional was the most accurate for TD-DFT calculations of

absorption spectra and first excitation energies. Correlation equations were derived for both cases.

This optimized method was used to evaluate the new HTM molecules shown in **Figure 5**. HOMO and LUMO energies of the new structures were obtained by calculating GSOP and ESOP values. The reorganization energies of the holes and electrons were also calculated. It was found that all the new structures, except BDT with HOMO of -5.48 eV, had suitable energy levels for HTM. Among them, Fl had the lowest reorganization energy for holes and the highest reorganization energy for electrons, along with HOMO of -5.39 eV and LUMO of -2.49 eV, making it the most promising HTM. Overall, the work has shown that by using reference data to optimize the computational methodology, choosing appropriate functionals, and properly correlating theoretical and experimental data, we can obtain reasonably accurate estimates for HOMO and LUMO. This allows us to accurately predict the properties of new materials and efficiently develop new HTMs.

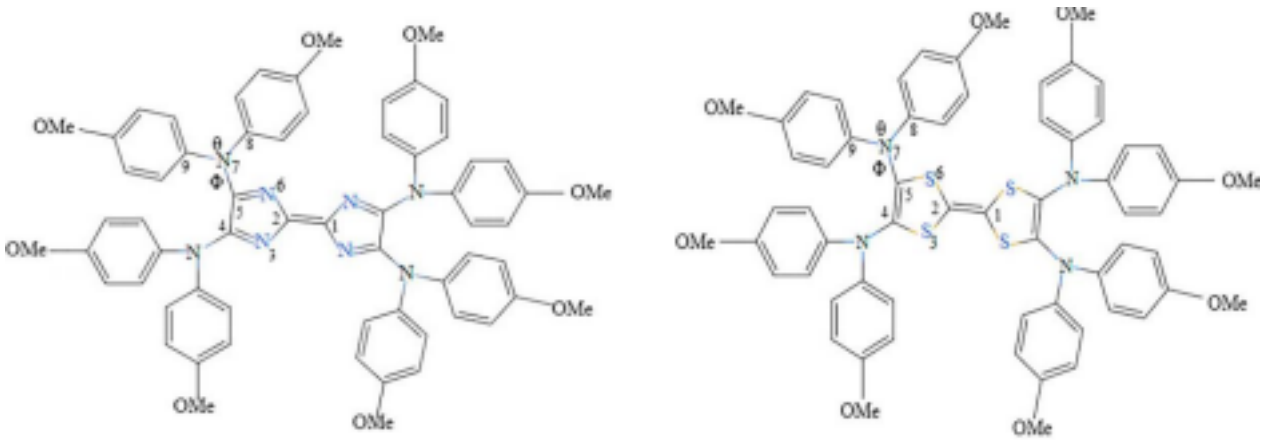

Figure 6. TAF-OMeTAD and TTF-OMeTAD derivatives. [24]

In 2018, Ashassi-Sorkhabi and Salehi-Abar used a computational approach to modify the core of Spiro-OMeTAD and develop two new HTMs that have better performance while being easier to synthesize than the original Spiro-OMeTAD [24]. The structures of the derivatives are shown in **Figure 6**. Initially, the structures were optimized with the B3LYP functional, while the HOMO energies were calculated with four different functionals: B3LYP, PBE0, PBE33 and PBE38. TD-DFT The calculations were performed with B3LYP, PBE0 and PBE38. The theoretical values were compared with the experimental values of reference spiro-OMeTAD. It was found that the PBE38 functional gave the most accurate HOMO energy, while the TD results of the PBE0 functional were

in good agreement with the experimental value. The charge transport properties of the derivatives were also investigated. The HOMO and LUMO energies of both derivatives were calculated to be in agreement with the valence and conduction bands of the perovskite, as they were slightly lower than those of the spiro-OMeTAD. The calculated hole mobilities showed that TTF-OMeTAD (tetrathiafulvalene-OMeTAD) had too low a mobility to function as a good HTM. TAF-OMeTAD (tetraazafulvalene-OMeTAD), on the other hand, had slightly lower hole mobility than spiro OMeTAD, which made it a potential HTM. However, because the theoretical methodology was not thoroughly optimized, such as the lack of more than one reference molecule and the small number of functionals studied, the results on the new derivatives are less accurate and reliable than they otherwise would have been. Nevertheless, it has been suggested that the core of Spiro-OMeTAD could be altered. This could be a promising direction for further work, as such an approach could help us to obtain the advantages of HTMs based on Spiro-OMeTAD while reducing the cost of synthesizing such HTMs.

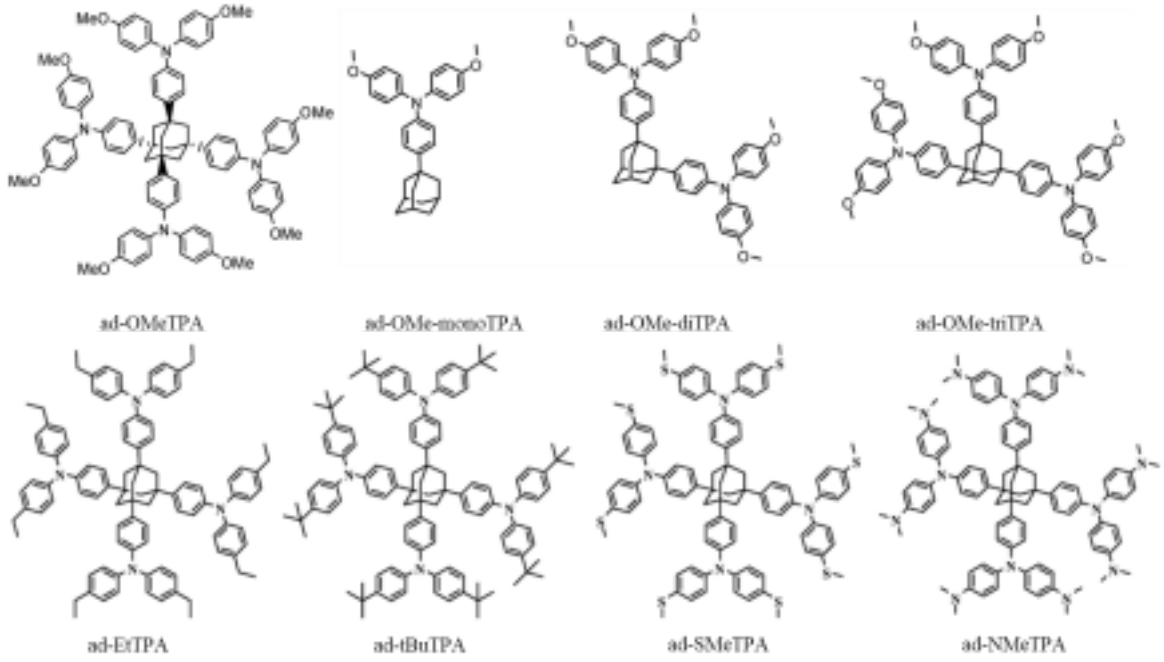

Figure 7. Adamantane-based novel HTMs. [25]

Similar to their previous work, Gapol and Kim calculated GSOP in 2019 to estimate the HOMO energy level of adamantane-based structures shown in **Figure 7** [25]. Four adamantane-based molecules and Spiro-OMeTAD were used as reference molecules. Six different functionals were used

for geometry optimization and GSOP calculations: B3LYP, APF, BHandHLYP, SOGGA11X, LC -ωPBE, and CAM -B3LYP. For the calculations of TD-DFT, three functionals were evaluated: B3LYP, SOGGA11X, and CAM -B3LYP. Comparison of the theoretical data with experimental data available for reference molecules showed that the CAM -B3LYP functional was the best for optimization and GSOP calculations, while B3LYP was the best for TD-DFT calculations. The ad-OMeTPA and ad EtTPA structures showed suitable properties to be promising HTMs, as they had the lowest reorganization energies for holes and the HOMO level of -4.863 eV and -5.176 eV, respectively. In addition, electrostatic potential maps (ESP) were constructed for the new HTMs to investigate the relationship between the reorganization energy of the holes and ESP. It was found that the larger contribution of the external substituent to the HOMO level also corresponds to larger geometric distortions during hole transfer and thus a larger reorganization energy λ. In addition, the ESP maps of the cationic shapes can be used to identify the regions of the molecule that experience the largest geometric distortions during hole transfer. In this way, it can be determined which parts of the molecule lead to greater hole reorganization energy and should be modified to increase hole mobility.

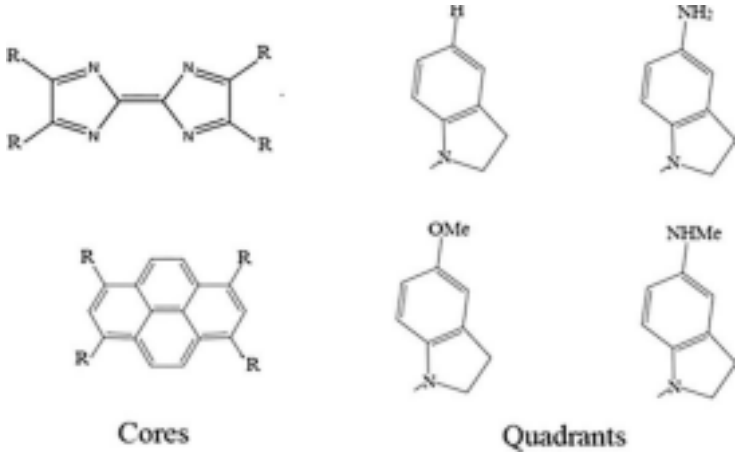

Figure 8. Indoline-based proposed HTMs. [26]

In the same year, Ashassi-Sorkhabi *et al.* reported that they used computational methods to study the effect of electron-donating groups on the properties of indoline substituents [26]. However, the authors did not thoroughly optimize the theoretical methodology. They used B3LYP to optimize the structures shown in **Figure 8**, PBE38 to calculate the energy levels of HOMO, and PBE0 for the

calculations of TD-DFT, based on their previous work [24] . Although this makes the calculated absolute values less accurate and reliable, they can still be analyzed in relation to each other and the

effects of the electron-donating groups can be studied. The authors report that for both nuclei, the addition of electron donating groups increases both the HOMO and LUMO energy levels, making them less negative compared to hydrogen substituted structures. Although for both hydrogen substituted structures it was calculated that the HOMO level is lower than the valence band of the perovskite, making them inefficient HTMs, all other structures with electron-donating substituents have energy levels that are properly aligned with the perovskite. However, no correlation was observed between the electron-donating ability of a substituent and the hole mobility values of HTMs.

3. Methodology

It has been shown that the ground state oxidation potential (GSOP) calculation yields a value closer to the experimental HOMO energy than the direct calculation of HOMO [22,23,25]. There are two approximate methods for determining the GSOP, shown in **Figure 9**: calculating the vertical energy difference ($GSOP_v$) (**Equation 1**) between neutral (E(M)) and oxidized ($E^+(M)$) molecules with neutral ground state geometries, and the calculation of the adiabatic energy difference ($GSOP_{a,}$) (**Equation 2**) between neutral (E(M)) and cationic ($E^+(M^+)$) geometries [22].

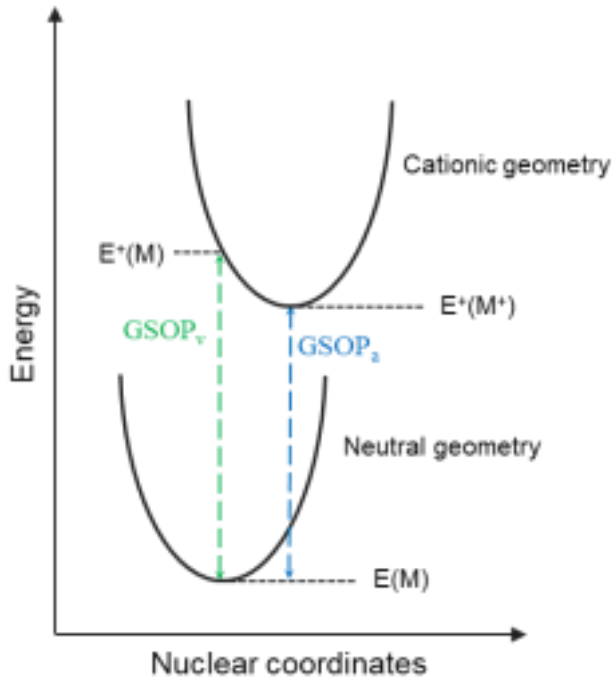

Figure 9. Schematic representation of $GSOP_v$ and $GSOP_a$.

$$GSOP_v = E(M) - E^+(M) \quad \textbf{(1)}$$

$$GSOP_a = E(M) - E^+(M^+) \quad \textbf{(2)}$$

Some studies have shown that the GSOPa method is generally more accurate than the $GSOP_v$ method because it provides values that are closer to the experimental HOMO energy values [22]. However, here we applied both methods as well as the direct calculation of the theoretical $HOMO_{calc}$ and compared three different results with the experimental $HOMO_{exp}$ values of the reference molecules (**Figure 10**).

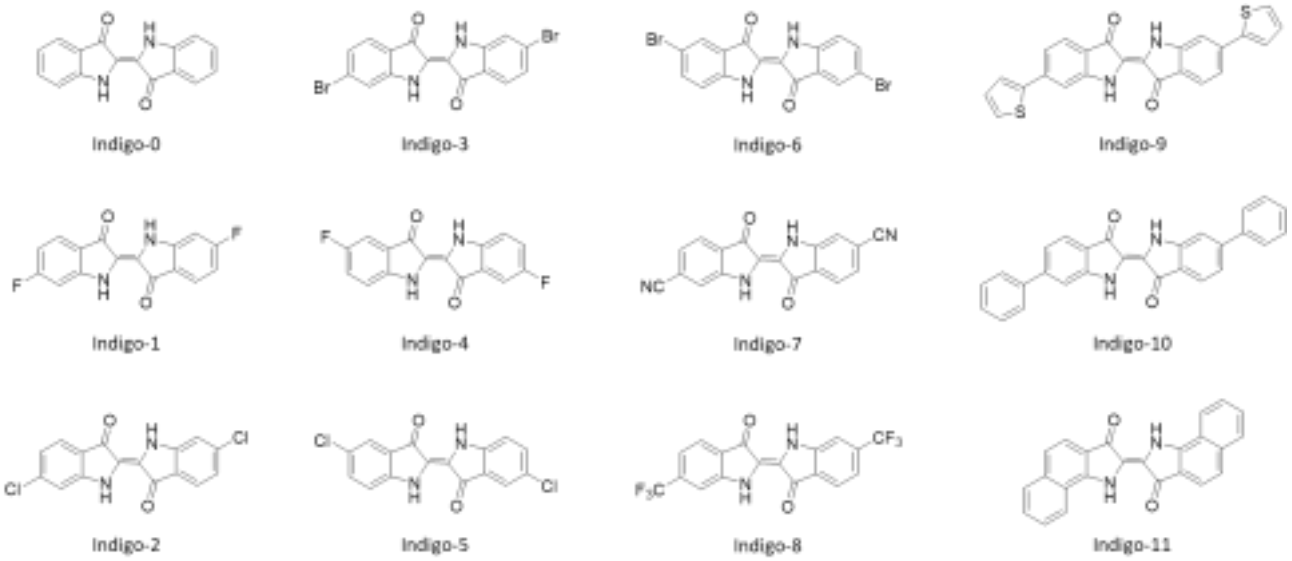

Figure 10. Reference indigo-based structures.

A more accurate method has also been used to evaluate newly designed structures. The excited state oxidation potential (ESOP), corresponding to the LUMO, was determined by adding the first excitation energy (E_1) to the GSOP. The hopping model and Marcus theory [27] were applied to describe the hole transport process in HTM. The hole reorganization energies (λ_h) were calculated using **Equation 3**:

$$\lambda_h = \lambda^+ + \lambda^0 = [E^+(M) - E^+(M^+)] + [E(M^+) - E(M)] \quad \textbf{(3)}$$

Chemical hardness was used to evaluate the chemical stability of the new molecules. Chemical hardness (η), as described by Parr and Pearson [28], describes the resistance of the chemical energy of a system to change and is calculated as follows (**Equation 4**):

$$\eta = \frac{1}{2}(I - A) \quad \textbf{(4)}$$

where I is the ionization energy and A is electron affinity. Since I corresponds to the negative of HOMO, it was determined from the negative of the corrected GSOP value, and A was calculated vertically based on **Equation 5**.

$$A = E(N) - E^-(N) \quad \textbf{(5)}$$

where $E^-(M)$ is an energy of reduced (anionic) molecule with neutral ground-state geometry.

To evaluate the accuracy of the theoretical method, the calculated values of $GSOP_v$, $GSOP_a$, $HOMO_{calc}$ were correlated with the experimental values of $HOMO_{exp}$ using regression analysis. Before building the estimation model, the mean absolute error (MAE) of the raw theoretical values was calculated. To build estimation models, a simple linear model was used to fit the theoretical data to the experimental values, and a regression equation was created. The mean square error (MSE) was used to compare the accuracy of the estimates. The method with the lowest MSE was used for further calculations. Residual plots were created and analyzed to check the data set for outliers, and the Cook distance, a measure of the influence of a single point on the regression, was calculated for each data point. In the case of an observed trend or outlier in the residual plot, a highly influential point with a Cook's D value greater than 1.0 was removed from the data set for a specific type of calculation.

The Gaussian 16 software [29] was used for all calculations. Five functionals were used to calculate $HOMO_{calc}$, $GSOP_a$, and $GSOP_v$, which were compared with $HOMO_{exp}$ of the reference structures: APFD, B3LYP, M06-2X, ωB97XD, and LC-ωHPBE. The 6-31G(d,p) basis set was used for all calculations. The geometries were optimized in the gas phase, while the single point energy calculations were performed with solvation effects in acetonitrile used in the measurement of $HOMO_{exp}$ [30,31], using a conduction-like polarized continuum model (C- PCM). Similarly, TD-DFT calculations were performed with solvation effects in 1,2-dichlorobenzene used in the measurement of the experimental optical bandgap (E_g) [30,31]. The best functional was then used for the optimization and calculation of the GSOP of the newly proposed structures. For the TD calculations, five functionals were used to calculate the E_1 values, which were compared and correlated with the experimental band gaps (E_g) of reference molecules: B3LYP, CAM -B3LYP, M06-2X, ωB97XD, and

LC -ωHPBE. The best functional in this step was further used to perform TD calculations for optimized proposed structures. Frequency calculations of the optimized neutral ground state geometries of all structures were performed to confirm that no imaginary frequency was observed.

4. Results and Discussion

4.1. Benchmarking theoretical methodology

$HOMO_{calc}$, $GSOP_a$, and $GSOP_v$ of the reference structures were computed with five different functionals and are listed in **Table 1**. For all functionals and references, the $GSOP_v$ values are closest to the experimental values, indicating that the vertical approach is generally more accurate than the adiabatic and direct approaches. The mean absolute error for the GSOPv calculations is 0.27 eV, while it is higher for $GSOP_a$ and $HOMO_{calc}$ at 0.41 and 0.76 eV, respectively. Among the five functionals, the long-range corrected LC -ωHPBE functional yields the smallest MAE of 0.10 eV in the calculation of $GSOP_v$, indicating that this combination of functional and vertical approach is the most accurate.

The superior accuracy of LC-ωHPBE functional with vertical approach was also confirmed by better correlation of $GSOP_v$ with the $HOMO_{exp}$, compared to $GSOP_a$ and $HOMO_{calc}$. All values calculated from five functionals over three approaches were correlated with experimental values to obtain a regression line and parameters to estimate $HOMO_{exp}$. The $GSOP_v$ values calculated with LC ωHPBE indeed estimate the experimental data better than the other methods, yielding the lowest MSE of 3.15×10^{-4}. On the other hand, $GSOP_a$ of LC-ωHPBE yielded an MSE of of 4.22×10^{-4}, and the direct $HOMO_{calc}$ provides less accurate estimates with an MSE of 4.67×10^{-4}. A similar trend was observed for the other two functionals, M06-2X and ωB97XD, with the calculated $GSOP_v$ leading to a better estimate of the experimental data than $GSOP_a$ and $HOMO_{calc}$. Interestingly, the order of $GSOP_v$ < $GSOP_a$ < $HOMO_{calc}$ for the MSE values was not the same when APFD and B3LYP functionals are used. For B3LYP functional, $GSOP_a$ produced the lowest MSE of 6.23×10^{-4}, and $GSOP_v$ resulted in the worst estimation, MSE of 6.58×10^{-4}. In contrast, for APFD functional, the $HOMO_{calc}$ and $GSOP_v$ calculations yield virtually the same quality of estimate with MSE values of $6.02\times10^{-4}$and 6.03×10^{-4}, respectively. while $GSOP_a$ yields the highest MSE value of all methods at 7.51×10^{-4}. With the lowest MAE and MSE, the calculation of $GSOP_v$ by LC-ωHPBE proved to be the most accurate method for estimating the HOMO energy.

Table 1. GSOPs and $HOMO_{calc}$ of reference structures calculated with different functionals, in eV.

Structure	Exp	APFD			B3LYP			M06-2X			wB97XD		
		$GSOP_a$	$GSOP_v$	$HOMO_{calc}$	$GSOP_a$	$GSOP_v$	$HOMO_{calc}$	$GSOP_a$	$GSOP_v$	$HOMO_{calc}$	$GSOP_a$	$GSOP_v$	HOM$_{calc}$
Indigo-0	-5.77	-5.26	-5.36	-5.54	-5.16	-5.25	-5.33	-5.38	-5.55	-6.51	-5.29	-5.45	-7.1

Indigo-1	-5.88	-5.40	-5.51	-5.68	-5.30	-5.40	-5.48	-5.53	-5.71	-6.68	-5.44	-5.61	-7.3
Indigo-2	-5.88	-5.45	-5.55	-5.74	-5.35	-5.45	-5.54	-5.57	-5.74	-6.72	-5.48	-5.65	-7.3
Indigo-3	-5.88	-5.45	-5.55	-5.74	-5.34	-5.44	-5.53	-5.57	-5.74	-6.72	-5.48	-5.65	-7.3
Indigo-4	-5.77	-5.29	-5.38	-5.55	-5.19	-5.28	-5.36	-5.42	-5.57	-6.53	-5.33	-5.48	-7.1
Indigo-5	-5.83	-5.40	-5.49	-5.67	-5.30	-5.39	-5.48	-5.53	-5.68	-6.64	-5.45	-5.60	-7.3
Indigo-6	-5.83	-5.49	-5.49	-5.67	-5.30	-5.38	-5.47	-5.54	-5.69	-6.64	-5.46	-5.61	-7.3
Indigo-7	-5.90	-5.59	-5.70	-5.88	-5.48	-5.58	-5.67	-5.68	-5.85	-6.83	-5.59	-5.76	-7.5
Indigo-8	-5.85	-5.50	-5.59	-5.77	-5.40	-5.48	-5.57	-5.62	-5.77	-6.74	-5.52	-5.67	-7.4
Indigo-9	-5.77	-5.28	-5.39	-5.58	-5.16	-5.26	-5.37	-5.43	-5.60	-6.58	-5.34	-5.51	-7.2
Indigo-10	-5.79	-5.27	-5.37	-5.56	-5.15	-5.25	-5.35	-5.40	-5.57	-6.55	-5.31	-5.47	-7.2
Indigo-11	-5.83	-5.31	-5.38	-5.57	-5.18	-5.25	-5.35	-5.50	-5.64	-6.54	-5.42	-5.55	-7.2
MAE		0.44	0.35	0.17	0.56	0.46	0.37	0.32	0.16	0.81	0.41	0.25	1.4
MSE		7.51×10^{-4}	6.03×10^{-4}	6.02×10^{-4}	6.23×10^{-4}	6.58×10^{-4}	6.26×10^{-4}	4.62×10^{-4}	4.01×10^{-4}	5.38×10^{-4}	4.79×10^{-4}	4.02×10^{-4}	$5.42\times$ 4

These results are in partial agreement with the results of Gapol *et al.* [22], where the LC -ωPBE functional, an earlier version of LC -ωHPBE, was found to be the most accurate after benchmarking with different reference structures. However, in contrast to our results, Gapol *et al.* found that the adiabatic approach had a better correlation with the experimental data than the vertical approach. This discrepancy can be explained by the fact that different core structures and references were used for benchmarking. Since the adiabatic approach accounts for geometric relaxations upon oxidation, the fact that it was more accurate in the case of the TBP-based structures suggests that these structures do indeed undergo geometric changes that can have significant effects on the energetics of these molecules. In contrast, the indigoids studied in this work have a more rigid indigo core due to conjugation and hydrogen bonding, suggesting that such structures are unlikely to undergo major geometric changes upon oxidation. Therefore, the vertical approach to calculating GSOP is more appropriate for these types of structures. This shows that neither the vertical nor the

adiabatic approach is universal and that for different structures, one of the two approaches may be more accurate. Therefore, a rigorous selection and evaluation of the theoretical methodology is always required for these types of calculations.

For the new structures, only GSOPv was calculated using LC -ωHPBE. The corrected GSOP was obtained from GSOPv using the correlation **Equation 6**:

$$GSOP = 0.5257 \times GSOP_v - 2.8188 \quad \textbf{(6)}$$

A similar benchmarking procedure was performed for the calculations of the first excitation energies, E_1. To obtain the LUMOs, the E_1 of the optimized reference structures were calculated using the method TD-DFT. Five functionals were used to calculate the E_1 of the reference structures and compare them with the experimental optical band gaps. The obtained initial values are summarized in **Table 2.**

Table 2. Experimental and theoretical first excitation energy (E_1) of 12 reference structures, in eV.

Structure	Experimental	B3LYP	CAM B3LYP	M06-2X	ωB97XD	LC ωHPBE	Cook's D*
Indigo-0	**2.07**	2.13	2.41	2.38	2.41	2.68	1.81×10^{-2}
Indigo-1	**2.36**	2.26	2.53	2.51	2.53	2.72	4.98
Indigo-2	**2.14**	2.18	2.45	2.43	2.45	2.64	4.58×10^{-2}
Indigo-3	**2.13**	2.18	2.44	2.42	2.44	2.63	2.78×10^{-2}
Indigo-4	**2.01**	2.03	2.32	2.30	2.32	2.59	4.53×10^{-1}
Indigo-5	**2.02**	2.07	2.37	2.34	2.37	2.65	8.98×10^{-3}
Indigo-6	**2.06**	2.06	2.37	2.33	2.37	2.57	1.32×10^{-2}

Indigo-7	**2.01**	2.04	2.33	2.31	2.33	2.52	1.48×10^{-1}
Indigo-8	**2.05**	2.11	2.38	2.36	2.38	2.56	1.15×10^{-5}
Indigo-9	**2.04**	2.11	2.40	2.38	2.41	2.59	9.50×10^{-2}
Indigo-10	**2.06**	2.12	2.41	2.38	2.41	2.60	3.25×10^{-2}
Indigo-11	**2.07**	2.05	2.38	2.34	2.40	2.57	2.11×10^{-3}
Mean Absolute Error		0.05	0.32	0.29	0.32	0.53	
Mean Squared Error		2.44×10^{-3}	1.64×10^{-3}	1.65×10^{-3}	1.59×10^{-3}	5.26×10^{-3}	

*- Cook's D for values calculated with ωB97XD functional are presented

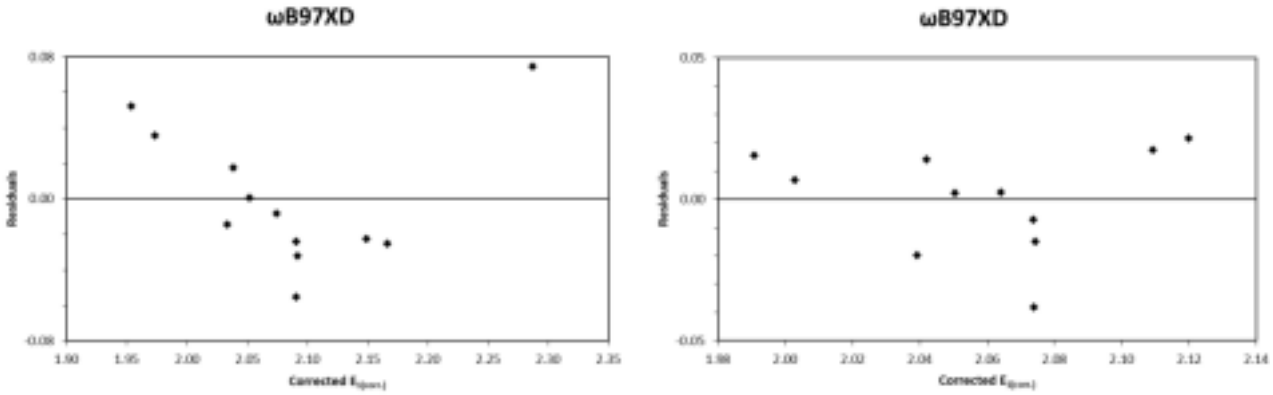

Figure 11. Residual plot before (left) and after (right) removal of outlier, ωB97XD functional.

When the calculated data were correlated with the experimental data, relatively high MSE values were obtained, which were an order of magnitude higher than the MSE of the GSOP calculations. To investigate the poor quality of the estimate and confirm the absence of bias and anomalies, residual plots were constructed. As can be seen in **Figure 11**, there is a clear downward trend in the residuals, indicating a nonlinear relationship, as well as a point far from the rest - possibly an outlier. To check the sample for an outlier, Cook's distance was calculated for each reference structure, which describes the influence of a point on the regression parameters [32]. As can be seen in **Table 2**, Cook's D was much higher for the Indigo-1 structure, the same outlier point in the residual plot, than for the other references and exceeded the rest by at least an order of

magnitude. These observations suggest that reference Indigo-1 is an outlier and should be excluded from the sample for TD calculations to obtain better estimates. After Indigo-1 was removed, the residual plots showed random scatter with no other outliers, and the MSE values decreased significantly. The final calculated values can be found in **Table 3**.

Table 3. Experimental and theoretical E_1 of reference structures, in eV.

Structure	Experimental	B3LYP	CAM B3LYP	M06-2X	wB97XD	LC-wHPBE
Indigo-0	**2.07**	2.13	2.41	2.38	2.41	2.68
Indigo-2	**2.14**	2.18	2.45	2.43	2.45	2.64
Indigo-3	**2.13**	2.18	2.44	2.42	2.44	2.63
Indigo-4	**2.01**	2.03	2.32	2.30	2.32	2.59
Indigo-5	**2.02**	2.07	2.37	2.34	2.37	2.65
Indigo-6	**2.06**	2.06	2.37	2.33	2.37	2.57
Indigo-7	**2.01**	2.04	2.33	2.31	2.33	2.52
Indigo-8	**2.05**	2.11	2.38	2.36	2.38	2.56
Indigo-9	**2.04**	2.11	2.40	2.38	2.41	2.59
Indigo-10	**2.06**	2.12	2.41	2.38	2.41	2.60
Indigo-11	**2.07**	2.05	2.38	2.34	2.40	2.57
Mean Absolute Error		**0.04**	0.33	0.30	0.33	0.54
Mean Squared Error		6.05×10^{-4}	3.92×10^{-4}	3.90×10^{-4}	$\mathbf{3.75\times10^{-4}}$	17.5×10^{-4}

The smallest MAE was obtained by using the B3LYP functional, 0.04 eV. Although the extremely small MAE indicates high accuracy of the B3LYP functional, the directional errors are inconsistent because it underestimates the value for two references while overestimating it for other references. This inconsistency is also reflected in the poor correlation of the calculated data with the experimental data, resulting in an MSE of 6.05×10^{-4}. Therefore, the estimate of the corrected $E_{1(corr.)}$ with the B3LYP functional is less accurate than the values calculated with other functionals. A notable exception is the LC -ωHPBE functional, which performs very poorly in TD calculations. It

has both the highest MAE of 0.53 eV and an MSE of 1.75×10^{-3}, indicating that it is not suitable for this type of calculation. In contrast, the ωB97XD functional gives the lowest MSE of 3.75×10^{-4}, indicating the most accurate estimate, so it was used in further TD calculations. The corrected E1(corr.) is obtained from the E_1 calculated with ωB97XD by the following correlation **Equation 7**:

$$E_{1(corr.)} = 0.9515\times E_1 - 0.2147 \quad \textbf{(7)}$$

Subsequently, the ESOP was calculated as follows:

$$ESOP = GSOP + E_{1(corr.)} \quad \textbf{(8)}$$

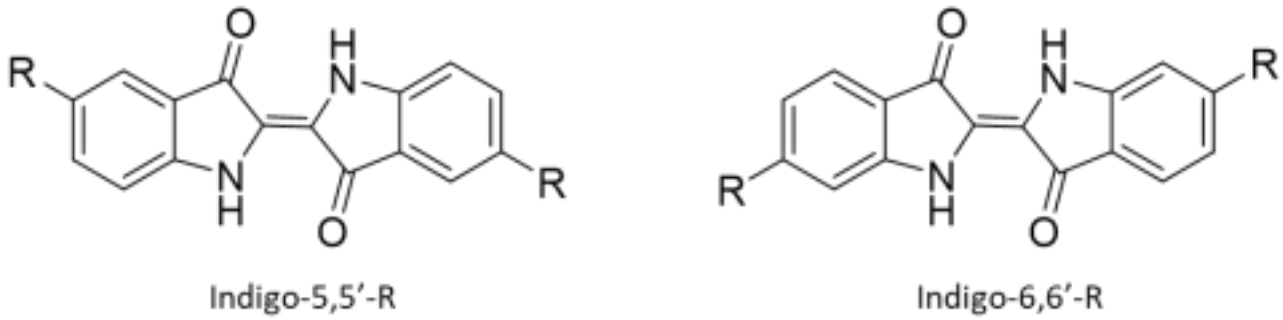

Figure 12. Two ways of substituents attachment.

4.2. Substituents positioning

Once the most accurate functionals were determined, new indigo-based structures were designed and calculated. Two main ways of inserting substituents into the indigo core structure were investigated, as shown in **Figure 12**. Various electron-donating and electron-withdrawing substituents were placed at the R positions: -OMe, -NMe2, -SMe, and -COOMe. Previous studies have shown that

electron donating groups increase the energy level of HOMO [21,26]. Since the highest HOMO is -5.77 eV, it was hypothesized that the addition of electron-donating groups would increase HOMO to make the structures more suitable for HTMs. However, the dependence of the influence of the substituent on its position for the indigo nucleus was not yet clear.

The calculated and corrected values of GSOP, $E_{1(corr.)}$, and ESOP of the new structures are shown in **Table 4**. As expected, electron-donating groups increase GSOP, while

electron-withdrawing groups decrease it, confirming the original hypothesis. However, the effect strongly depends on the position of the bond of a group. The dimethylamine group increases the GSOP to a greater extent than the methoxy group because it donates more electrons, up to -5.54 eV, which corresponds to an increase of 0.23 compared to the -5.77 eV of indigo [30] when it is in the 5.5' position. In the 6.6' position, the effect is much less pronounced, increasing the GSOP by only 0.08 eV. On the other hand, the methoxy group in the 5,5'-position reaches -5.65 eV, which corresponds to a difference of 0.12 eV and is thus almost twice as effective as dimethylamine. Virtually no change is observed in the 6,6'-position. In contrast, electron-withdrawing groups lower the GSOP by up to 0.13 eV and reach -5.90 eV for the carboxyl group in the 5.5' position. From the obtained results, it appears that a substituent at the 5,5'- position, as in indigo-5,5'-R, has a greater influence on the energy of HOMO of the molecule than at the 6,6'-position. This is true for both electron-donating and electron-attracting groups, as we can see that electron-donating groups are more effective at increasing GSOP at the 5.5' position, while electron-attracting groups are more effective at decreasing GSOP at the 5.5' position. This difference was attributed to the composition of HOMO of the indigo core. The contribution of carbon atoms at the 6,6' positions to HOMO of the molecule is minimal, as shown in **Figure 13**. Therefore, the addition of any group at these positions has a smaller effect on the energy of the resulting HOMO, since the contribution of the substituent would also be minimal. Small changes of HOMO can still be obtained at the 6,6' positions due to the indirect influence of the substituents by inductive effects. In contrast, the carbon atoms at the 5,5' positions contribute significantly to HOMO, allowing the substituents to interact directly with HOMO of the molecule, making these positions suitable for the evolution of the energetics of the molecule. This shows that the bonding position of the substituents is very important and that the HOMO of a core structure can be studied first to successfully develop new organic materials for various applications.

Table 4. Calculated parameters of structures with electron-donating and withdrawing groups, in eV.

Structure	GSOP	$E_{1(corr.)}$	ESOP
Indigo-5,5'-OMe	-5.65	1.89	-3.76
Indigo-6,6'-OMe	-5.77	2.21	-3.56

Indigo-5,5'-NMe2	-5.54	1.76	-3.78
Indigo-6,6'-NMe2	-5.69	2.26	-3.43
Indigo-5,5'-SMe	-5.84	2.09	-3.75
Indigo-6,6'-SMe	-5.79	2.13	-3.66
Indigo-5,5'-COOMe	-5.90	2.14	-3.76
Indigo-6,6'-COOMe	-5.83	1.98	-3.85

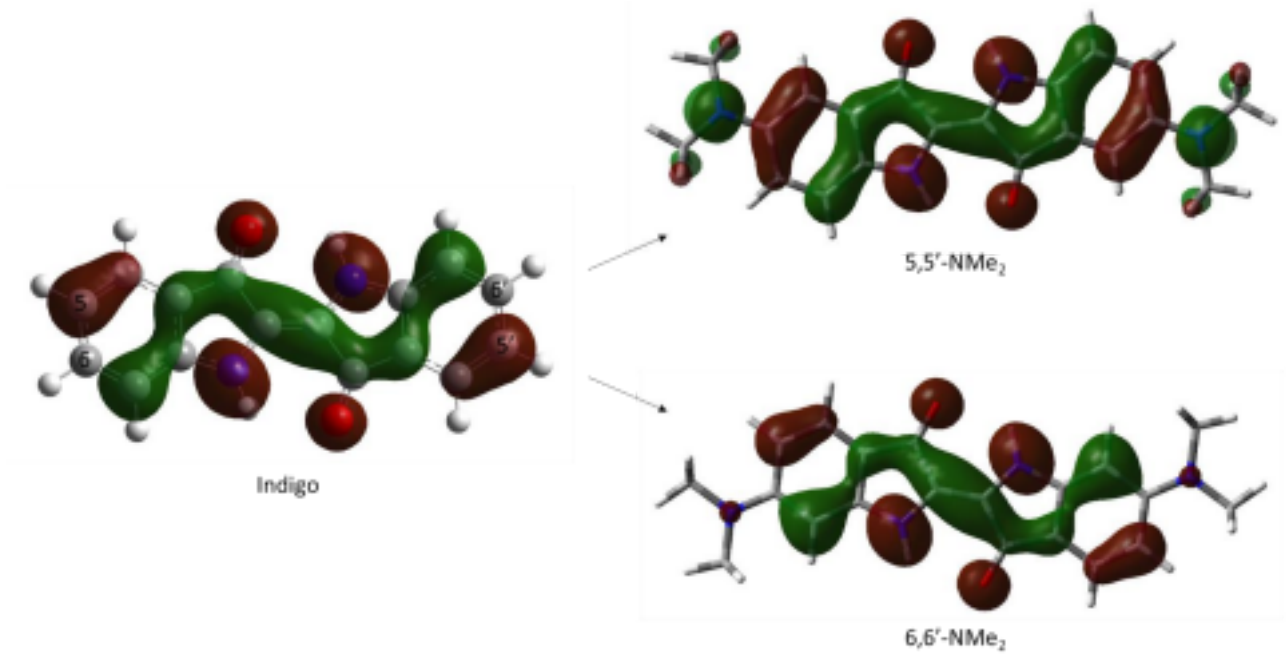

Figure 13. HOMO of the indigo and two ways of substitution.

This principle can be applied to explain differences in reference structures, especially when halogens are attached to the indigo nucleus. Since the halogens were attached in both ways, we can see different effects on HOMO of indigoids [30]. It is known that halogens act as both electron-

donating and electron-attracting groups by different mechanisms. Due to lone pairs, they can donate electron density and thus increase the energy of HOMO. On the other hand, due to their high electronegativity, they also withdraw electron density from carbon through the polar effect and decrease the energy of HOMO. The reference structures indigo-1-3 are halogenated at the 6,6' positions, while indigo-4-6 are halogenated at the 5,5' positions. At the 6,6' positions, all electron

donating effects on the energy of HOMO are greatly diminished due to the small contribution to HOMO, while the inductive electron-withdrawing effect can still take place. Since the inductive effect is less pronounced, the differences in electronegativity between fluorine and the other halogens do not affect the result, leading to the same HOMO of -5.88 eV for all three halogens. In contrast, a direct contribution to HOMO occurs at the 5.5' positions, and the electron-donating effects of the halogens counteract the electron-withdrawing forces. Therefore, the energies of HOMO of 6,6'-halogenated indigoids are less negative, -5.83 eV. Fluorine has a stronger electron donation than chlorine or bromine due to a much shorter bond length and better overlap with HOMO of the indigo nucleus. Therefore, it further increases the energy of HOMO and completely offsets the electron withdrawal, resulting in an unchanged energy of -5.77 eV. Overall, electron-withdrawing effects predominate for the halogens, with the exception of fluorine, resulting in a decreased energy of HOMO. The extent to which the energy decreases depends on the position of the bond.

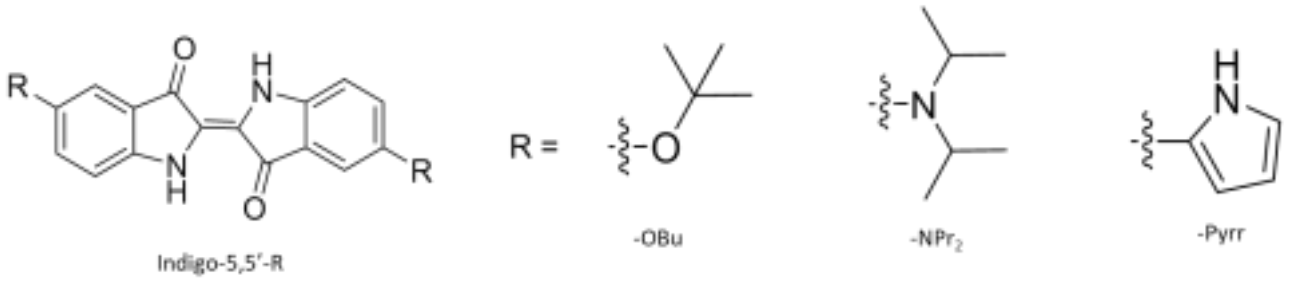

Figure 14. New substituents at 5,5'-positions.

4.3. New structures at 5,5'-positions

Based on the results from the previous section, it was decided to introduce new substituents at 5,5'-positions. The focus was on electron-donating groups because they increase GSOP, which is desirable for our goals. In particular, the groups - OR and -NR_2 have been shown to be effective substituents. Therefore, these groups were modified with more bulky alkyl-R groups to avoid

aggregation of neighboring molecules in HTM. In addition, asymmetric structures with the groups - OR and -NR_2 on one side and bulky cyclic groups on the other side of the indigo core were investigated to achieve the electron donating and HOMO energy enhancing effects while creating steric hindrances between neighboring molecules by cyclic groups (**Figure 14**).

Table 5. Calculated parameters of new indigoid HTMs, in eV.

Structure	GSOP	$E_{1(corr.)}$	ESOP	λ_h	η
Indigo-5,5'-OMe	-5.65	1.89	-3.76	0.40	1.29
Indigo-6,6'-OMe	-5.77	2.21	-3.56	0.52	1.44
Indigo-5,5'-NMe2	-5.54	1.76	-3.78	0.62	1.29
Indigo-6,6'-NMe2	-5.69	2.26	-3.43	0.54	1.52
Indigo-5,5'-SMe	-5.84	2.09	-3.75	0.59	1.33
Indigo-6,6'-SMe	-5.79	2.13	-3.66	0.49	1.37
Indigo-5,5'-COOMe	-5.90	2.14	-3.76	0.50	1.33
Indigo-6,6'-COOMe	-5.83	1.98	-3.85	0.46	1.26
Indigo-5,5'-OBu	-5.63	1.87	-3.76	0.40	1.30
Indigo-5,5'-NPr_2	-5.57	1.79	-3.78	0.73	1.30
Indigo-5-NMe_2-5'- Pyrr	-5.55	1.83	-3.72	0.60	1.26

The LC-ωHPBE was used to calculate the new structures. TD The calculations were performed using the ωB97XD// LC -ωHPBE functional. **Equations 7, 8,** and **9** were used to obtain corrected GSOP, $E_{1(corr.)}$ and ESOP values, respectively. Since a vertical approach was used to calculate GSOP, the electron affinity *A* was also calculated vertically using **Equation 6**. **Equations 4 and 5** were used to obtain hole reorganization energies and chemical hardness values. The results are summarized in **Table 5**.

Since lead-based PSCs pose environmental and health safety issues, this work focuses on the lead-free and mixed-metal perovskites. Among lead-free perovskites, tin-based structures show promise due to similar size and properties of tin and lead, suggesting potential applicability of $MASnI_3$

[9,10] and $CsSnI_3$ [11,12] in PSCs. On the other hand, mixed-metal perovskite $MASn_{0.5}Pb_{0.5}I_3$ [13]

shows high photocurrent, good PCE and lowered amounts of toxic lead, making it a good candidate for photovoltaic applications. Therefore, new HTMs were designed for application in tin-based and mixed-metal PSCs.

As shown from **Table 5**, the structures with simple electron donating groups, -OR and -NR_2, have a higher placed GSOP. When the isopropyl and tert-butyl groups become more bulky compared to the methyl group, the energies of the resulting structures do not change significantly, at most by 0.03 eV. This means that some degree of steric hindrance can be introduced without losing the electron donating and energy increasing effects. As **Figure 15** shows, structures with bulky alkyls, indigo-5,5'-OBu and indigo-5,5'-NPr_2, as well as planar indigo-5,5'-OMe and indigo-5,5'-NMe_2 structures are energetically suitable for $CsSnI_3$-based PSCs because their GSOP and ESOP are higher than VB and CB of the perovskite, namely -5.69 and -4.38 eV [33]. Among the two classes -OR and -NR_2 - the indigo-5,5'- OR structures have a lower GSOP, so they would lead to lower voltage losses during charge transfer and therefore produce a higher open circuit voltage (V_{oc}). On the other hand, the difference between the GSOP of indigo-5,5'-OMe (-OBu) and VB of $CsSnI_3$ is only 0.04 (0.06) eV. Such a small barrier could lead to a higher rate of charge recombination and reduce the short circuit current (J_{sc}). The two structures have similar ESOP energy levels, suggesting that the energy barrier blocking negative charge carriers is equally effective, which would reduce the charge recombination and increase the J_{sc}. At the same time, the asymmetric indigo-5-NMe_2-5'-Pyrr has a very similar GSOP to indigo-5,5'-NMe_2 (-5.55 and -5.54 eV), even higher than the GSOP of indigo 5,5'-NPr_2 (-5.57 eV). This may suggest that creating an asymmetric molecule with a cyclic substituent on one side is a better strategy for introducing steric hindrance while maintaining a high GSOP than modifying the -NR_2 group.

In addition, indigo-5,5'-OMe and -OBu exhibit lower hole reorganization energies ($\lambda_h = 0.40$ eV), suggesting that they may have better hole mobility than indigo-5,5'-NMe_2 ($\lambda_h = 0.62$ eV) and -NPr_2 ($\lambda_h = 0.73$ eV). On the other hand, indigo-5-NMe_2-5'-Pyrr lowers λ_h (0.60 eV), compared to indigo-5,5'-NMe_2, while -NPr_2 increases it. The asymmetric structure maintains the high GSOP and also improves the mobility of the holes.

Indigo-5,5'-OMe and indigo-5,5'-NMe_2 appear to be equally stable because their hardness values are the same ($\eta = 1.29$ eV). Substitution of the methyl group with bulky alkyl groups does not seem to affect the stability significantly, if not slightly improve it, since the hardness is increased by

0.01 eV ($\eta = 1.30$ eV) in both cases. On the other hand, the introduction of a cyclic group into the asymmetric molecule seems to decrease the stability as the hardness decreases ($\eta = 1.26$ eV). The

high GSOP and better hole mobility of the asymmetric structure come at the cost of lower stability. However, the changes in hardness of 0.01-0.03 eV are very small and can be considered negligible.

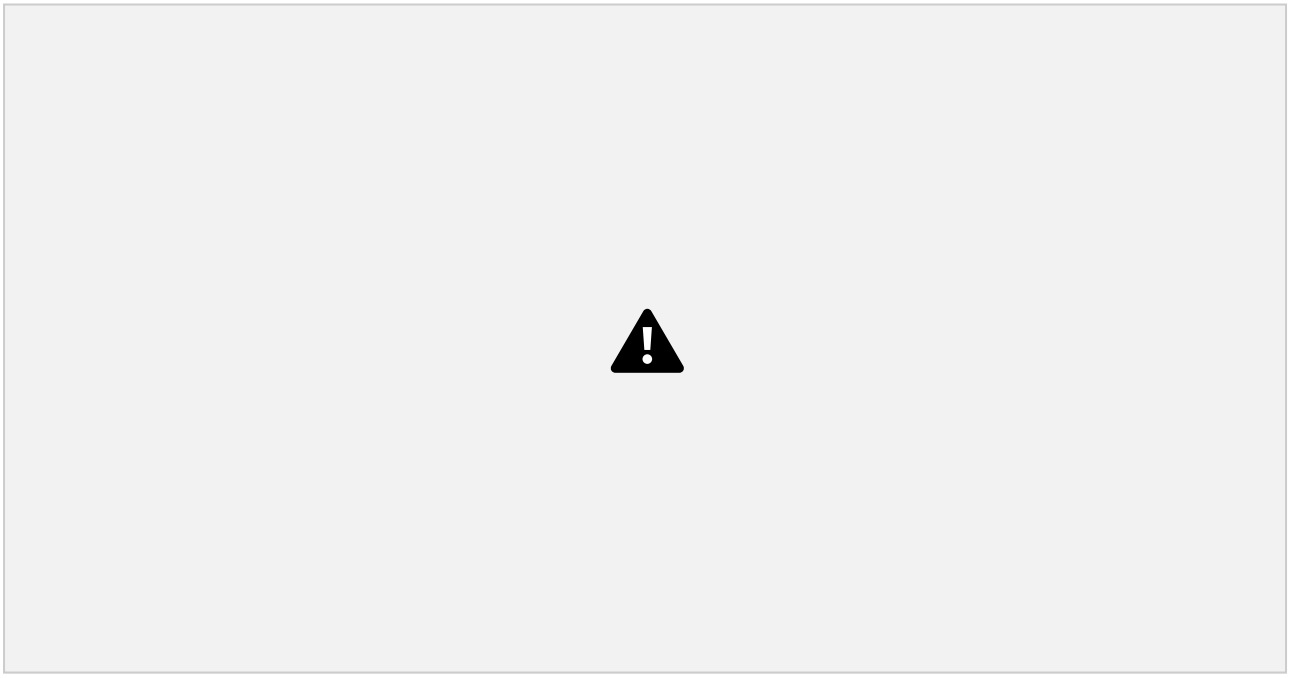

Figure 15. Alignment of the new structures with perovskites.

Based on these results, indigo-5,5'- OR, indigo-5,5'-NR_2 and asymmetric indigo-5-NMe_2-5'-Pyrr could serve as HTMs for $CsSnI_3$-based PSCs, where indigo-5,5'- OR would likely lead to better photovoltaic parameters due to better hole mobility. On the other hand, only indigo-5.5'-NR_2 and indigo-5-NMe_2-5'-Pyrr structures would work as HTMs for $MASn_{0.5}Pb_{0.5}I_3$ mixed metal PSCs. As shown in **Figure 15**, only amine-based structures have a GSOP suitable for valence band (VB) of $MASn_{0.5}Pb_{0.5}I_3$ (-5.61 eV [13]). Alkoxy structures have too low GSOP, which would lead to inefficient hole extraction. Among amine-based structures, the asymmetric molecule is the optimal one because it has a high GSOP and a lower reorganization energy for holes than symmetric amine-based molecules. The steric hindrances introduced by the substitution of methyl with butyl for indigo-5,5'- OBu and the cyclic group of the asymmetric structure are expected to prevent unwanted aggregation of molecules and charge recombination in HTM.

Both the indigo 5,5'- OR and indigo 5,5'-NR_2 structures and the asymmetric indigo 5-NMe_2 5'-Pyrr structures should be good alternatives to spiro-OMeTAD because the new structures have a lower GSOP than HOMO of spiro-OMeTAD (-5.22 eV [34]), which would lead to higher V_{oc}, and

the stability problems associated with spiro-OMeTAD HTM [10,13] are solved by using indigoid HTMs for $CsSnI_3$ and $MASn_{0.5}Pb_{0.5}I_3$ PSCs.

5. Conclusion

New indigoid structures were computationally designed and proposed as potential HTMs for tin- and mixed-metal-based PSCs. DFT and TD-DFT were used to calculate the properties of the new indigoids, including GSOP, E_1, ESOP, hole reorganization energies, and chemical hardness. Several functions were compared using twelve reference structures to determine the most accurate for calculating indigoid structures. It was found that the $GSOP_v$ calculation gave the best agreement with the experimental data. LC-ωHPBE functional was found to be the most suitable for $GSOP_v$ calculation and ωB97XD was found to be the most suitable for TD calculations. The influence of substituent positioning on HOMO energy was demonstrated. It was found that the attachment of electron donating groups at 5,5' positions of the indigo increased the HOMO more effectively than at 6,6' positions, which should be taken into account in the development of new indigoids.

Among the new indigo-based structures, indigo-5,5'-OMe, indigo-5,5'-OBu, indigo-5,5'-NMe_2, indigo-5,5'-NPr_2, and indigo-5-NMe_2-5'-Pyrr were found to be suitable for use as HTMs for $CsSnI_3$ PSCs. On the other hand, for $MASn_{0.5}Pb_{0.5}I_3$ PSCs, only indigo-5.5'-NMe_2, indigo-5.5'-NPr_2 and indigo-5-NMe_2-5'-Pyrr can be used as HTMs. Indigo-5,5'-OBu, indigo-5,5'-NPr_2, and indigo-5-NMe_2-5'-Pyrr are expected to have lower charge recombination rates due to steric hindrances introduced by bulky groups. In addition, these indigoids have a deeper HOMO than spiro-OMeTAD, which should lead to a higher V_{oc}. In general, it appears that indigoids have the potential to be used as HTMs because they match the bands of perovskites and gold electrodes. Therefore, they should be considered for synthesis and experimental application as HTMs for PSCs.

References

[1] A. Kojima, K. Teshima, Y. Shirai, T. Miyasaka, Organometal halide perovskites as visible-light sensitizers for photovoltaic cells, J. Am. Chem. Soc. 131 (2009) 6050–6051.

[2] H. Min, D.Y. Lee, J. Kim, G. Kim, K.S. Lee, J. Kim, M.J. Paik, Y.K. Kim, K.S. Kim, M.G. Kim, T.J. Shin, S. Il Seok, Perovskite solar cells with atomically coherent interlayers on SnO2 electrodes, Nature. 598 (2021) 444–450.

[3] T.M. Brenner, D.A. Egger, L. Kronik, G. Hodes, D. Cahen, Hybrid organic - Inorganic perovskites: Low-cost semiconductors with intriguing charge-transport properties, Nat. Rev. Mater. 1 (2016) 1–16.

[4] A.K. Jena, A. Kulkarni, T. Miyasaka, Halide Perovskite Photovoltaics: Background, Status, and Future Prospects, Chem. Rev. 119 (2019) 3036–3103.

[5] H.S. Kim, C.R. Lee, J.H. Im, K.B. Lee, T. Moehl, A. Marchioro, S.J. Moon, R. Humphry-Baker, J.H. Yum, J.E. Moser, M. Grätzel, N.G. Park, Lead iodide perovskite sensitized all-solid-state submicron thin film mesoscopic solar cell with efficiency exceeding 9%, Sci. Rep. 2 (2012) 1–7.

[6] M.M. Lee, J. Teuscher, T. Miyasaka, T.N. Murakami, H.J. Snaith, Efficient Hybrid Solar Cells Based on Meso-Superstructured Organometal Halide Perovskites, Science. 338 (2012) 643–647.

[7] M. Liu, M.B. Johnston, H.J. Snaith, Efficient planar heterojunction perovskite solar cells by vapour deposition, Nature. 501 (2013) 395–398.

[8] G. Flora, D. Gupta, A. Tiwari, Toxicity of lead: A review with recent updates, Interdiscip. Toxicol. 5 (2012) 47–58.

[9] F. Hao, C.C. Stoumpos, D.H. Cao, R.P.H. Chang, M.G. Kanatzidis, Lead-free solid-state organic inorganic halide perovskite solar cells, Nat. Photonics. 8 (2014) 489–494.

[10] N.K. Noel, S.D. Stranks, A. Abate, C. Wehrenfennig, S. Guarnera, A.A. Haghighirad, A. Sadhanala, G.E. Eperon, S.K. Pathak, M.B. Johnston, A. Petrozza, L.M. Herz, H.J. Snaith, Lead-free organic inorganic tin halide perovskites for photovoltaic applications, Energy Environ. Sci. 7 (2014) 3061–3068.

[11] M.H. Kumar, S. Dharani, W.L. Leong, P.P. Boix, R.R. Prabhakar, T. Baikie, C. Shi, H. Ding, R. Ramesh, M. Asta, M. Graetzel, S.G. Mhaisalkar, N. Mathews, Lead-free halide perovskite solar cells with high photocurrents realized through vacancy modulation, Adv. Mater. 26 (2014) 7122–7127.

[12] L.J. Chen, C.R. Lee, Y.J. Chuang, Z.H. Wu, C. Chen, Synthesis and Optical Properties of Lead-Free Cesium Tin Halide Perovskite Quantum Rods with High-Performance Solar Cell Application, J. Phys. Chem. Lett. 7 (2016) 5028–5035.

[13] F. Hao, C.C. Stoumpos, R.P.H. Chang, M.G. Kanatzidis, Anomalous band gap behavior in mixed Sn and Pb perovskites enables broadening of absorption spectrum in solar cells, J. Am. Chem. Soc. 136 (2014) 8094–8099.

[14] Z. Hawash, L.K. Ono, Y. Qi, Recent Advances in Spiro-MeOTAD Hole Transport Material and Its Applications in Organic–Inorganic Halide Perovskite Solar Cells, Adv. Mater. Interfaces. 5 (2018).

[15] J.Y. Seo, H.S. Kim, S. Akin, M. Stojanovic, E. Simon, M. Fleischer, A. Hagfeldt, S.M. Zakeeruddin, M. Grätzel, Novel p-dopant toward highly efficient and stable perovskite solar cells, Energy Environ. Sci. 11 (2018) 2985–2992.

[16] B. Cai, Y. Xing, Z. Yang, W.H. Zhang, J. Qiu, High performance hybrid solar cells sensitized by organolead halide perovskites, Energy Environ. Sci. 6 (2013) 1480–1485.

[17] S. Ryu, J.H. Noh, N.J. Jeon, Y. Chan Kim, W.S. Yang, J. Seo, S. Il Seok, Voltage output of efficient perovskite solar cells with high open-circuit voltage and fill factor, Energy Environ. Sci. 7 (2014) 2614–2618.

[18] J.H. Heo, H.J. Han, D. Kim, T.K. Ahn, S.H. Im, Hysteresis-less inverted CH3NH3PbI3 planar perovskite hybrid solar cells with 18.1% power conversion efficiency, Energy Environ. Sci. 8 (2015) 1602–1608.

[19] F. Cai, J. Cai, L. Yang, W. Li, R.S. Gurney, H. Yi, A. Iraqi, D. Liu, T. Wang, Molecular engineering of conjugated polymers for efficient hole transport and defect passivation in perovskite solar cells, Nano Energy. 45 (2018) 28–36.

[20] K. Jiang, J. Wang, F. Wu, Q. Xue, Q. Yao, J. Zhang, Y. Chen, G. Zhang, Z. Zhu, H. Yan, L. Zhu, H.L. Yip, Dopant-Free Organic Hole-Transporting Material for Efficient and Stable Inverted All-Inorganic and Hybrid Perovskite Solar Cells, Adv. Mater. 32 (2020) 1–7.

[21] W.J. Chi, Z.S. Li, The theoretical investigation on the 4-(4-phenyl-4-α-naphthylbutadieny)-triphenylamine derivatives as hole transporting materials for perovskite-type solar cells, Phys. Chem. Chem. Phys. 17 (2015) 5991–5998.

[22] M.A.B. Gapol, M.P. Balanay, D.H. Kim, Molecular Engineering of Tetraphenylbenzidine-Based Hole Transport Material for Perovskite Solar Cell, J. Phys. Chem. A. 121 (2017) 1371–1380.

[23] M. Pastore, S. Fantacci, F. De Angelis, Ab initio determination of ground and excited state oxidation potentials of organic chromophores for dye-sensitized solar cells, J. Phys. Chem. C. 114 (2010) 22742–22750.

[24] H. Ashassi-Sorkhabi, P. Salehi-Abar, Design of two novel hole transport materials via replacing the core of spiro-OMeTAD with tetrathiafulvalene and tetraazafulvalene for application in perovskite solar cells, Sol. Energy. 173 (2018) 132–138.

[25] M.A.B. Gapol, D.H. Kim, Novel adamantane-based hole transport materials for perovskite solar cells: A computational approach, Phys. Chem. Chem. Phys. 21 (2019) 3857–3867.

[26] H. Ashassi-Sorkhabi, P. Salehi-Abar, A. Kazempour, Effect of electron-donating groups on the electrochemical and optical properties of indoline substituents as hole transport materials: A computational study, Sol. Energy. 180 (2019) 146–151.

[27] R.A. Marcus, Electron transfer reactions in chemistry. Theory and experiment, J. Electroanal. Chem. 438 (1997) 251–259.

[28] R.G. Parr, R.G. Pearson, Absolute Hardness: Companion Parameter to Absolute Electronegativity, J. Am. Chem. Soc. 105 (1983) 7512–7516.

[29] M.J. Frisch, G.W. Trucks, H.B. Schlegel, G.E. Scuseria, M. a. Robb, J.R. Cheeseman, G. Scalmani, V. Barone, G. a. Petersson, H. Nakatsuji, X. Li, M. Caricato, a. V. Marenich, J. Bloino, B.G. Janesko, R. Gomperts, B. Mennucci, H.P. Hratchian, J. V. Ortiz, a. F. Izmaylov, J.L. Sonnenberg, Williams, F. Ding, F. Lipparini, F. Egidi, J. Goings, B. Peng, A. Petrone, T. Henderson, D. Ranasinghe, V.G. Zakrzewski, J. Gao, N. Rega, G. Zheng, W. Liang, M. Hada, M. Ehara, K. Toyota, R. Fukuda, J. Hasegawa, M. Ishida, T. Nakajima, Y. Honda, O. Kitao, H. Nakai, T. Vreven, K. Throssell, J. a. Montgomery Jr., J.E. Peralta, F. Ogliaro, M.J. Bearpark, J.J. Heyd, E.N. Brothers, K.N. Kudin, V.N. Staroverov, T. a. Keith, R. Kobayashi, J. Normand, K. Raghavachari, a. P. Rendell, J.C. Burant, S.S. Iyengar, J. Tomasi, M. Cossi, J.M. Millam, M. Klene, C. Adamo, R. Cammi, J.W. Ochterski, R.L. Martin, K. Morokuma, O. Farkas, J.B. Foresman, D.J. Fox (2016) Gaussian 16, Revision C.01, Gaussian, Inc., Wallin.

[30] I. V. Klimovich, L.I. Leshanskaya, S.I. Troyanov, D. V. Anokhin, D. V. Novikov, A.A. Piryazev, D.A. Ivanov, N.N. Dremova, P.A. Troshin, Design of indigo derivatives as environment-friendly organic semiconductors for sustainable organic electronics, J. Mater. Chem. C. 2 (2014) 7621–7631.

[31] I. V. Klimovich, A. V. Zhilenkov, L.I. Kuznetsova, L.A. Frolova, O.R. Yamilova, S.I. Troyanov, K.A. Lyssenko, P.A. Troshin, Novel functionalized indigo derivatives for organic electronics, Dye. Pigment. 186 (2021) 108966.

[32] R.D. Cook, Detection of Influential Observation in Linear Regression, Technometrics. 19 (1977) 15–18.

[33] S. Tao, I. Schmidt, G. Brocks, J. Jiang, I. Tranca, K. Meerholz, S. Olthof, Absolute energy level positions in tin- and lead-based halide perovskites, Nat. Commun. 10 (2019) 1–10.

[34] T. Krishnamoorthy, F. Kunwu, P.P. Boix, H. Li, T.M. Koh, W.L. Leong, S. Powar, A. Grimsdale, M. Grätzel, N. Mathews, S.G. Mhaisalkar, A swivel-cruciform thiophene based hole-transporting material for efficient perovskite solar cells, J. Mater. Chem. A. 2 (2014) 6305–6309.